PAPER

Check for updates

Construction of nano-sized FOX-7/ZIF-8 composites for fast decomposition and reduced sensitivity†

Binshen Wang, ID *[a] Fangbao Jiao,[b] Rong Xu[b] and Hongzhen Li ID *[b]

Herein, novel nano-sized 1,1-diamino-2,2-dinitroethylene ($C_2H_4N_4O_4$, FOX-7)/zeolitic imidazolate framework-8 (ZIF-8) composites are constructed by facile liquid-assisted mechanochemical reactions. In contrast to two-step thermal decomposition of raw FOX-7, the prepared FOX-7/ZIF-8 composites demonstrate a single high-intensity exothermal decomposition attributed to the catalysis of ZIF-8. Benefiting from nano-sized energetic materials and the buffering effect of ZIF-8, the mechanical sensitives of FOX-7/ZIF-8 composites are decreased.

Energetic materials are a class of material with high amount of stored chemical energy that can be released.[1–3] They represent one of the crucial functional materials which are widely used in military and civil applications. According to their different uses, energetic materials can be classified as propellants, explosives, and pyrotechnics. Exploitation of novel energetic materials is a long-term strategic task, and the common requirements include high energy, low sensitivity, fast decomposition, easy preparation.

1,1-Diamino-2,2-dinitroethylene ($C_2H_4N_4O_4$, FOX-7) has received extensive attention as a high energy material with a density of 1.878 g cm^{-3} and a heat of formation of 133.7 kJ mol^{-1} since it was synthesized firstly by Latypov *et al.* in 1998.[4–8] Pioneering researches have been continuously carried out on fabrication of FOX-7 based composites to modify its properties for practical applications. Klapötke *et al.* reported FOX-7 hosted in MFI-type zeolite for detection purposes.[9,10] Huang *et al.* studied the FOX-7 embedded in mesoporous carbon FDU-15, showing the extreme insensitivity close to that of FDU-15.[11] Fu *et al.* constructed nano graphene oxide–metal–FOX-7 composites to promote complete thermal decomposition of FOX-7.[12] Li *et al.* prepared FOX-7/F_{2602} PBX[13] and FOX-7/viton microspheres[14] with improved thermal stability. Some formulations containing FOX-7 exhibited good application performance in the field of solid propellant.[12,15,16] However, FOX-7 and most its composites undergo two-steps thermal decomposition

at gradually elevated temperature, which is markedly different from other high energy materials, such as 1,3,5-trinitro-1,3,5-triazine (RDX), 1,3,5,7-tetranitro-1,3,5,7-tetrazocine (HMX), hexanitrohexaazaisowurtzitane (CL-20). Compared with single-step process, two-steps decomposition tends to reduce the energy release efficiency of FOX-7, and increase the energy loss. Hence, design and construction of FOX-7 based composites, that can convert two-steps decomposition into a single-step process, is desired for developing novel solid propellants.

Metal–organic frameworks (MOFs), emerging as a representative class of crystalline porous materials with adjustable pore structure, regular channels, abundant interaction sites, diverse composition, attract a surge of attention to be hosting matrixes for host–guest chemistry.[17–19] An attractive aspect of MOF materials lies in the facts that they not only can retain the individual functions, but also often exhibit novel properties derived from blending of the individuals.[20] Benefiting from the abundant nano-sized cavities and regular pores, MOFs host can act as confinement to avoid the aggregation of guest molecules. Encapsulation of FOX-7 within the pores of MOFs may provide a promising way to construct nano-sized energetic materials, which showed decreased sensitivities compared with micro-sized ones.[21,22] Additionally, metal species and organic linkers of MOFs host would participate in the thermal decomposition of guest, thus it is expected to regulate decomposition process of FOX-7.

In this work, we report a utilization of a liquid-assisted mechanochemical route for the construction of FOX-7/MOF composite materials. Liquid-assisted mechanochemical milling was conducted as an alternative to the conventional solution-based strategy because of its priority in composition control of guest species and size reduction effect.[23–25] A chemically stable zeolitic imidazolate framework-8 (ZIF-8) was used as prototype MOF material due to its easy and efficient preparation

aInstitute of New Energy and Low-Carbon Technology, Sichuan University, Chengdu, Sichuan 610207, China. E-mail: wangbinshen@scu.edu.cn

bInstitute of Chemical Materials, China Academy of Engineering Physics (CAEP), Mianyang, Sichuan 621900, China. E-mail: hongzhenli@caep.cn

process. The resulting FOX-7/ZIF-8 composites were completely characterized by FT-IR, powder X-ray diffraction analysis (XRD), nitrogen adsorption/desorption measurements, and scanning electron microscopy (SEM). Furthermore, the thermal behaviour and mechanical sensitivities of these composites were investigated.

The FOX-7/ZIF-8 composites were prepared by easily liquid-assisted mechanochemical reactions (Scheme 1). Commercial $Zn(OH)_2$ powder was used as the zinc source to react with 2-methylimidazole (HMeIM) in the presence of FOX-7 at room temperature for 4 h. During this process, FOX-7 *in situ* merged with generated ZIF-8. After washing with ethanol and drying, homogeneous yellow powders were generated as desired composites. To investigate the effect of the proportions of FOX-7 to ZIF-8 on the properties of the obtained FOX-7/ZIF-8 composites, various molar ratios of FOX-7 to $Zn(OH)_2$, HMeIM were used as starting materials, and the resulting materials were named as FOX-7/ZIF-8 (I) [FOX-7 : $Zn(OH)_2$: HMeIM = 1 : 1 : 8], FOX-7/ZIF-8 (II) [FOX-7 : $Zn(OH)_2$: HMeIM = 1 : 1.5 : 12], FOX-7/ZIF-8 (III) [FOX-7 : $Zn(OH)_2$: HMeIM = 1 : 2 : 16], respectively.
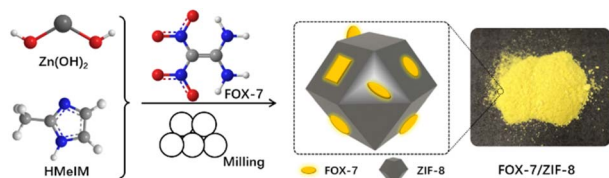
The FT-IR spectra of FOX-7/ZIF-8 composites were shown in Fig. 1a. The peaks at ~3406, ~3298, ~1636 cm^{-1} were ascribed to the $-NH_2$, and the peaks at ~1524, ~1472 cm^{-1} were related to the $-NO_2$ of FOX-7.[26] The peaks at ~1308, ~1145 cm^{-1} could be attributed to the C–N bands in the imidazole groups,[27] and the peaks at ~760, ~692 cm^{-1} demonstrated the presence of the Zn–O and Zn–N bonds.[28] The existence of these peaks proved the successful assembly of FOX-7, zinc and HMeIM. XRD was performed to examine the crystallinity of the composites (Fig. 1b). The characteristic peaks at $2\theta = 7.3°$, $10.4°$, $12.7°$, $14.8°$, $16.4°$ were corresponding to 110, 200, 211, 220, and 310 planes of ZIF-8, respectively.[29] The presence of these strong peaks confirmed a high crystallinity of ZIF-8 in the structure of as-prepared FOX-7/ZIF-8 composites. The peaks observed at $2\theta = 20.1°$, $26.8°$, $28.1°$ supported the presence of FOX-7 with good crystallinity, which are assigned to its 111, 020, 021 planes, respectively.[14,30] The elemental analysis results showed the content of FOX-7 in composites gradually decreased in FOX-7/ZIF-8 (I) to FOX-7/ZIF-8 (III) (Table S1†).

Nitrogen sorption isotherms were collected at 77 K to evaluate the porosity of liquid-assisted mechanochemically prepared ZIF-8 and FOX-7/ZIF-8 composites (Fig. 1c and S1†). All samples displayed type-IV isotherms. Owing to the space-occupying of FOX-7 in the cages of ZIF-8, the Brunauer–Emmett–Teller (BET) surface areas decreased from 1110 m^2 g^{-1} (ZIF-8) to 921 m^2 g^{-1} [FOX-7/ZIF-8 (III)], 868 m^2 g^{-1} [FOX-7/ZIF-8

(II)], 659 m^2 g^{-1} [FOX-7/ZIF-8 (I)], respectively (Table S2†). SEM image of liquid-assisted mechanochemically prepared ZIF-8 exhibited roughly dodecahedron structure with relatively uniform distribution of crystal particle size (Fig. S2†). For FOX-7/ZIF-8 composites, the SEM images showed the ordered structure of ZIF-8 was remained mostly (Fig. 1d–f). And some particles were distributed around ZIF-8 due to the presence of FOX-7 in nanoscale size. These results indicated the structural integrity of the ZIF-8 framework with introduction of nano-sized FOX-7. The presence of ZIF-8 was expected to improve the stability of composites due to its buffering effect.

The thermal behaviour of FOX-7/ZIF-8 composites were studied by using differential scanning calorimetry (DSC) measurements at a heating rate of 5 °C min^{-1} (Fig. 2). Particularly, raw FOX-7 was used as a control. As the temperate was increased above 200 °C, all samples underwent decomposition without melting. DSC thermogram of pure FOX-7 exhibited two decomposition steps. The initial decomposition peak was observed at ~223 °C, which was attributed to the emergence of nitro-to-nitrite rearrangement and the destruction of conjugated system and hydrogen bonds.[31] And the second exothermal peak at ~283 °C was ascribed to the fracture of carbon skeleton in FOX-7 molecule. In contrast, the DSC thermogram of FOX-7/ZIF-8 (I) indicated a single high-intensity exothermal peak at ~206 °C. The peak intensity was much greater than each exothermal peak of FOX-7. It demonstrated the catalytic effect of ZIF-8 on the exothermic decomposition of FOX-7. Converting two-steps decomposition into single-step is conducive to improving the energy release efficiency and reducing the energy loss in the exothermic process of energetic materials. Analogously, the DSC thermogram of FOX-7/ZIF-8 (II) and FOX-7/ZIF-8 (III) also showed one-step decomposition peak at ~205 and ~202 °C, respectively. The gradual decrease in peak intensities were due to the reduction of FOX-7 content. Furthermore, equivalent physical mixture of FOX-7 and $Zn(OH)_2$ [denoted as FOX-7 + $Zn(OH)_2$] afforded two exothermic peaks similar to FOX-7 (Fig. S3†), and equivalent physical mixture of FOX-7 and ZIF-8 (denoted as FOX-7 + ZIF-8) afforded a single exothermic peak similar to FOX-7/ZIF-8 composites (Fig. S4†). It showed the unique catalytic effect of ZIF-8 beyond inorganic zinc salt.

To explore the possible microstructure of FOX-7/ZIF-8 composites and the reason for the difference of exothermic behaviour between raw FOX-7 and FOX-7/ZIF-8 composites, studies on structural modeling and *ab initio* molecular dynamics simulation (AIMD) were conducted. FOX-7 molecules were inserted into the cages of ZIF-8 according to appropriate density, affording proposed FOX-7/ZIF-8 Periodic cell structure with 3–4 FOX-7 molecules in each cage (Fig. 3a). The energy of the proposed FOX-7/ZIF-8 structure converged successfully through first-principles optimization, and the structural configuration was maintained through relaxation for 5 ps at 300 K. It demonstrated the thermodynamics and kinetics of the proposed FOX-7/ZIF-8 structure are stable. Notably, the FOX-7 molecules in the cages were no longer planar accumulation due to the van der Waals interactions with surrounding molecules in cages.

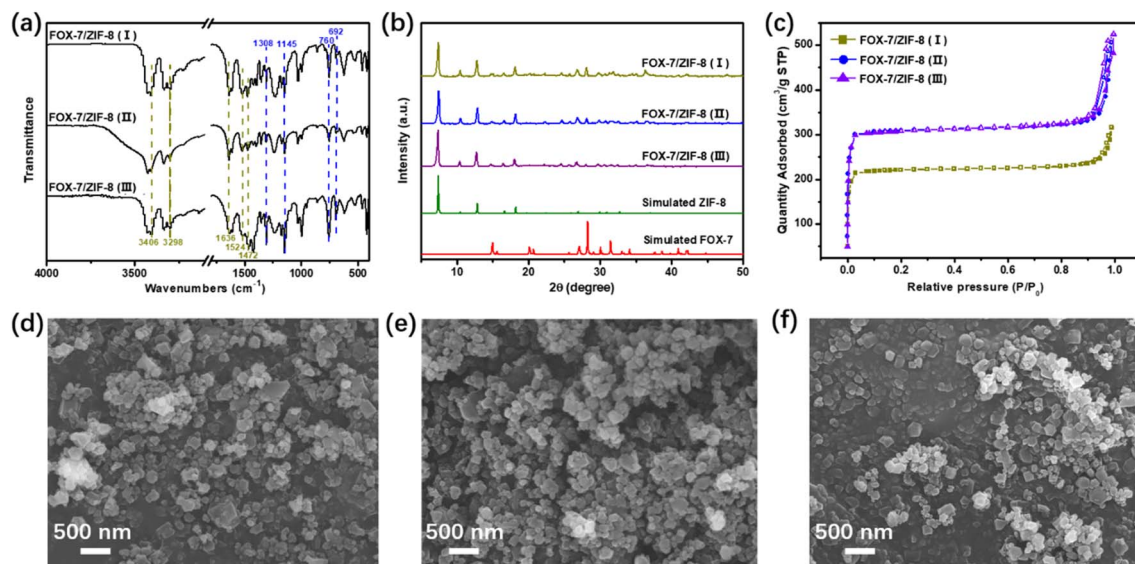**Scheme 1** Synthesis route for FOX-7/ZIF-8 composites.

Fig. 1 (a) IR spectra, (b) XRD patterns, (c) nitrogen adsorption/desorption isotherms of FOX-7/ZIF-8 composites. SEM images of (d) FOX-7/ZIF-8 (I), (e) FOX-7/ZIF-8 (II), (f) FOX-7/ZIF-8 (III).
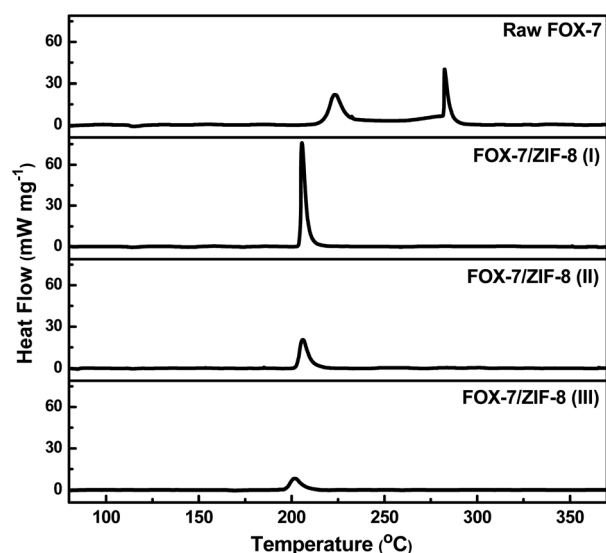

Fig. 2 DSC curves of raw FOX-7 and FOX-7/ZIF-8 composites at a heating rate of 5 °C min^{-1}.
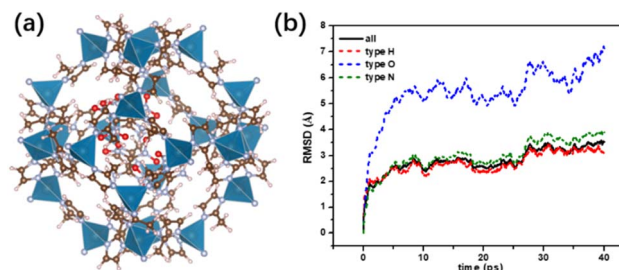

Fig. 3 (a) Schematic diagram of theoretical model structure of FOX-7/ZIF-8 composite, (b) Root Mean Square Deviation (RMSD) of atomic position shift in FOX-7/ZIF-8 model when temperature rises to 1000 K.

300–1000 K temperature programmed AIMD simulation of NVT ensemble for 40 ps were carried out for the proposed FOX-7/ZIF-8 composite structure and α-FOX-7. The reversible hydrogen transfer was observed in the heating process of FOX-7/ZIF-8 and α-FOX-7. It was generally believed that reversible hydrogen transfers consumed energy.[32] Thus, the higher frequency of reversible hydrogen transfers generally led to the higher the initial decomposition temperature. The frequency of reversible hydrogen transfers of α-FOX-7 was higher than that of FOX-7/ZIF-8. It preliminarily explains that raw FOX-7 had a higher thermal decomposition temperature than the FOX-7/ZIF-8 composites. Furthermore, the Root Mean Square Deviation (RMSD) diagram of FOX-7/ZIF-8 model showed oxygen

atom had significantly larger position shift compared with hydrogen atom and nitrogen atom (Fig. 3b). It indicated the rotation of –NO$_2$. In contrast, the position shift of oxygen atom in α-FOX-7 was slightly smaller than that of hydrogen atom, and slightly greater than that of nitrogen atom, which was caused by the vibration before denitrification (Fig. S5†). And the track file of FOX-7/ZIF-8 model during the heating process exhibited oxygen atom on the –NO$_2$ was attracted by Zn atom on the MOF structure, leading to deflection and separation of oxygen atom from the molecular plane. Based on these results, it was speculated that the initial thermal decomposition path of FOX-7 in cage of ZIF-8 was abscission of oxygen radicals from FOX-7 molecule and reaction with the transferred hydrogen in the system to form H$_2$O. It was different from the traditional thermal decomposition path of pure α-FOX-7 that denitrogenates led to rapid and centralized disassembly of the molecule structure.[33]

The mechanical sensitivities of FOX-7, FOX-7 + ZIF-8 and these FOX-7/ZIF-8 composites were further investigated, as shown in Table 1. The impact sensitivity (H_{50}) and friction

Table 1 Mechanical sensitivities of FOX-7/ZIF-8 composites

Compound	Impact sensitivity H_{50}/cm	Fraction sensitivity P/%
Raw FOX-7	50.0	28
FOX-7 + ZIF-8	62.3	100
FOX-7/ZIF-8 (I)	101.0	0
FOX-7/ZIF-8 (II)	>112.2	0
FOX-7/ZIF-8 (III)	>112.2	0

sensitivity (explosion probability, P) of FOX-7/ZIF-8 (I) are 101.0 cm, 0%, respectively. It was less sensitive to mechanical stimuli than raw FOX-7, FOX-7 + ZIF-8 and some other reported FOX-7 composites, such as FOX-7/F_{2602} PBX,[13] FOX-7/viton granules,[14] FOX-7/viton microspheres.[14] The reduced mechanical sensitivities were assumed to be due to nano-sized energetic materials and the buffering effect of ZIF-8. Moreover, the large specific surface area of FOX-7/ZIF-8 composites could accelerate the heat transfer process, and prevented the accumulation of heat and the formation of "hot spots".[13] H_{50} of FOX-7/ZIF-8 (II) and FOX-7/ZIF-8 (III) were >112.2 cm, and their P were 0%. These results indicated that assembly of FOX-7 and ZIF-8 provided a beneficial effect for improving the safety property of energetic materials.

In summary, this study demonstrated a facile and universal approach to synthesize FOX-7/ZIF-8 composites by *in situ* liquid-assisted mechanochemical reactions. The chemical composition and surface morphology of these composites were completely characterized. Benefiting from the abundant nano-sized cavities and regular pores of ZIF-8, the size of FOX-7 in composites were reduced to the nanoscale. Different from the two-steps thermal decomposition process of raw FOX-7, the FOX-7/ZIF-8 composites exhibited a single high-intensity exothermal decomposition due to the catalysis of ZIF-8. It is beneficial to improve the energy release efficiency and reduce the energy loss during the exothermic process of energetic materials. The microstructure of FOX-7/ZIF-8 composites was simulated by AIMD study, and the initial thermal decomposition path of FOX-7/ZIF-8 composites was abscission of oxygen radicals. Furthermore, all prepared FOX-7/ZIF-8 composites demonstrated lower sensitives than raw FOX-7 to mechanical stimuli attributed to nano-sized energetic materials and the buffering effect of ZIF-8. This work opens an avenue for functionalizing MOFs with energetic materials *via* host–guest chemistry, thus broadening the application scope of MOF materials.

Author contributions

H. Li designed the study, supervised the project, and revised the manuscript. B. Wang, F. Jiao and R. Xu performed materials synthesis and characterization. All authors discussed the results and contributed to the writing of the manuscript.

Conflicts of interest

There are no conflicts to declare.

Notes and references

1 P. Yin, Q. Zhang and J. n. M. Shreeve, *Acc. Chem. Res.*, 2016, **49**, 4–16.
2 J. C. Bennion and A. J. Matzger, *Acc. Chem. Res.*, 2021, **54**, 1699–1710.
3 S. Zhang, Q. Yang, X. Liu, X. Qu, Q. Wei, G. Xie, S. Chen and S. Gao, *Coord. Chem. Rev.*, 2016, **307**, 292–312.
4 N. V. Latypov, J. Bergman, A. Langlet, U. Wellmar and U. Bemm, *Tetrahedron*, 1998, **54**, 11525–11536.
5 A. J. Bellamy, in *High Energy Density Materials*, ed. T. M. Klapötke, Springer Berlin Heidelberg, Berlin, Heidelberg, 2007, ch. FOX-7 (1,1-diamino-2,2-dinitroethene), pp. 1–33.
6 Y. Zhang, Q. Sun, K. Xu, J. Song and F. Zhao, *Propellants, Explos., Pyrotech.*, 2016, **41**, 35–52.
7 D. S. Viswanath, T. K. Ghosh and V. M. Boddu, in *Emerging Energetic Materials: Synthesis, Physicochemical, and Detonation Properties*, Springer Netherlands, Dordrecht, 2018, ch. FOX-7 (1,1-diamino-2,2-dinitroethylene), pp. 101–139.
8 T. M. Klapöetke, B. Krumm, J. T. Lechner and J. Stierstorfer, *Dalton Trans.*, 2022, **51**, 5788–5791.
9 G. Majano, S. Mintova, T. Bein and T. M. Klapötke, *Adv. Mater.*, 2006, **18**, 2440–2443.
10 G. Majano, S. Mintova, T. Bein and T. M. Klapötke, *J. Phys. Chem. C*, 2007, **111**, 6694–6699.
11 H. Cai, L. Tian, B. Huang, G. Yang, D. Guan and H. Huang, *Microporous Mesoporous Mater.*, 2013, **170**, 20–25.
12 C. Zhang, X. Fu, X. Zhang, J. Li, X. Fan and G. Zhang, *Nanomaterials*, 2020, **10**, 144.
13 Y. Yang, X. Li, Y. Zhao, Y. Han, Y. Sun and J. Wang, *AIP Adv.*, 2021, **11**, 025323.
14 Y. Yang, X. Li, Y. Sun, Y. Zhao, Y. Han and J. Wang, *J. Energ. Mater.*, 2022, **40**, 358–374.
15 B. Florczak, *Cent. Eur. J. Energ. Mater.*, 2008, **5**, 103–111.
16 W. Xie, Y. Zhao, W. Zhang, Y. Liu, X. Fan, B. Wang, W. He and Q.-L. Yan, *Propellants, Explos., Pyrotech.*, 2018, **43**, 308–314.
17 M. Gutierrez, Y. Zhang and J.-C. Tan, *Chem. Rev.*, 2022, **122**, 10438–10483.
18 J.-S. Qin, S. Yuan, C. Lollar, J. Pang, A. Alsalme and H.-C. Zhou, *Chem. Commun.*, 2018, **54**, 4231–4249.
19 E. Gkaniatsou, C. Sicard, R. Ricoux, J.-P. Mahy, N. Steunou and C. Serre, *Mater. Horiz.*, 2017, **4**, 55–63.
20 C.-D. Wu and M. Zhao, *Adv. Mater.*, 2017, **29**, 1605446.
21 W. Pang, C. Deng, H. Li, L. T. DeLuca, D. Ouyang, H. Xu and X. Fan, *Nanomaterials*, 2022, **12**, 133.
22 R. Xu, C. An, H. Huang, J. Wang, B. Ye and B. Liu, *RSC Adv.*, 2019, **9**, 21042–21049.
23 M. S. El-Eskandarany, A. Al-Hazza, L. A. Al-Hajji, N. Ali, A. A. Al-Duweesh, M. Banyan and F. Al-Ajmi, *Nanomaterials*, 2021, **11**, 2484.

24 T. Friscic, C. Mottillo and H. M. Titi, *Angew. Chem., Int. Ed.*, 2020, **59**, 1018–1029.

25 S. L. James, C. J. Adams, C. Bolm, D. Braga, P. Collier, T. Friscic, F. Grepioni, K. D. M. Harris, G. Hyett, W. Jones, A. Krebs, J. Mack, L. Maini, A. G. Orpen, I. P. Parkin, W. C. Shearouse, J. W. Steed and D. C. Waddell, *Chem. Soc. Rev.*, 2012, **41**, 413–447.

26 M. Anniyappan, M. B. Talawar, G. M. Gore, S. Venugopalan and B. R. Gandhe, *J. Hazard. Mater.*, 2006, **137**, 812–819.

27 R. Bakhshali-Dehkordi and M. A. Ghasemzadeh, *J. Mol. Struct.*, 2021, **1236**, 130298.

28 L. Yang, B. Tang and P. Wu, *J. Mater. Chem. A*, 2015, **3**, 15838–15842.

29 Y. Ban, Z. Li, Y. Li, Y. Peng, H. Jin, W. Jiao, A. Guo, P. Wang, Q. Yang, C. Zhong and W. Yang, *Angew. Chem., Int. Ed.*, 2015, **54**, 15483–15487.

30 B. Gao, P. Wu, B. Huang, J. Wang, Z. Qiao, G. Yang and F. Nie, *New J. Chem.*, 2014, **38**, 2334–2341.

31 B. Huang, Z. Qiao, F. Nie, M. Cao, J. Su, H. Huang and C. Hu, *J. Hazard. Mater.*, 2010, **184**, 561–566.

32 J. Wang, Y. Xiong, H. Li and C. Zhang, *J. Phys. Chem. C*, 2018, **122**, 1109–1118.

33 A. Gindulyte, L. Massa, L. L. Huang and J. Karle, *J. Phys. Chem. A*, 1999, **103**, 11045–11051.